Supporting Information (SI)

SI1. Consideration of Non-linearity of Gas and Solutions for a Mixed Gas State

For gas flow, we can use a pseudo-pressure variable to linearize Eq. (1D) as μ and c_t are functions of pressure. Thee pseudo-pressure p_p is defined as (Haskett et al., 1988)

$$p_p = 2\int_{p_0}^{p} \frac{p}{\mu z}\, d\, p \qquad \text{(S1)}$$

By combining Eq. (S1) with the ideal gas law, the pseudo-density may be expressed as

$$\rho_p = \frac{pM}{RT} = \frac{p^2 M}{\mu z RT} \qquad \text{(S2)}$$

Because viscosity and compressibility do not change significantly (less than 0.7%) between 200 psi and atmospheric pressures, Eq. (S2) can be simplified to

$$\rho_p = \frac{p^2 M}{RT} \qquad \text{(S3)}$$

Thus, the density change is replaced by the pseudo-density for a precise calibration by using pressure squared.

During the GPT experiment, different gases in the reference and sample cells may complicate the hydrodynamic equilibrium of gas, and consequently the expression of transport phenomena, as the viscosity and gas compressibility are in a mixed state. Therefore, during the GPT experiment

when a different gas exists between the reference and sample cells a, a mixed viscosity should be used after the gas in reference cell is released into the sample cell. The viscosity of mixture μ_{mix} under pressure in Eqs. (3A)-(3C) can be calculated from (Brokaw, 1968; Sutherland, 1895)

$$\mu_{mix} = \sum \frac{\mu_i}{1+\frac{1}{y_i}(\sum_{\substack{j=1 \\ j\neq i}}^{n} B_{ij} y_j)} + \mu_p \qquad \text{(S4)}$$

B_{ij} is a correction parameter independent of gas composition and can be expressed as

$$B_{ij} = \frac{[1+(\frac{\mu_i}{\mu_j})^{0.5}(\frac{M_j}{M_i})^{0.5}]^2}{2\sqrt{2}(1+\frac{M_j}{M_i})^{0.5}} \qquad \text{(S5)}$$

in which μ_p is the correction term for the viscosity variation as its changes with pressure and given by

$$\mu_p = 1.1 \times 10^{-8}(e^{1.439\rho_{rm}} - e^{-1.111{\rho_{rm}}^{1.858}}) \times {M_m}^{0.5} \cdot \frac{{P_{cm}}^{2/3}}{{T_{cm}}^{1/6}} \qquad \text{(S6)}$$

SI2. Gas Transport in GPT

From Eq. (1D), the transport of gas in the GPT with the "unipore" model under a small pressure gradient in a spherical coordinate system with laminar flow is based on the Darcy-type relation. Because the transfer rate of the fluid is proportional to the concentration gradient, this process can be expressed as:

$$\frac{\partial \rho_p}{\partial t} = \frac{k}{c_t \phi_f \mu}(\frac{2}{r}\frac{\partial \rho_p}{\partial r} + \frac{\partial^2 \rho_p}{\partial r^2}) \qquad \text{(S7)}$$

We set

$$k_s = \frac{k}{\mu} \tag{S8}$$

$$K_a = \frac{k_s}{c_t \phi_f} \tag{S9}$$

Then, Eq. (S7) becomes:

$$\frac{\partial \rho_p}{\partial t} = K_a\left(\frac{2}{r}\frac{\partial \rho_p}{\partial r} + \frac{\partial^2 \rho_p}{\partial r^2}\right) \text{ or } \frac{\partial}{\partial t}(\rho_p r) = K_a \frac{\partial^2}{\partial r^2}(\rho_p r) \tag{S10}$$

We next introduce the following dimensionless variables:

$$U_s = \frac{r}{R}\frac{(\rho_{ps} - \rho_{p2})}{(\rho_{p0} - \rho_{p2})} \tag{S11}$$

$$U_f = \frac{\rho_{pf} - \rho_{p2}}{\rho_{p0} - \rho_{p2}} \tag{S12}$$

$$\xi = \frac{r}{R} \tag{S13}$$

$$\tau = \frac{K_a t}{R^2} \tag{S14}$$

where ρ_1 and ρ_2 are the gas density in the reference and sample cells, and ρ_0 is the gas density outside the connected pore volume (the gas has flowed from the reference into sample cells but not into samples), and ρ_0 is given by

$$\rho_0 = \frac{V_1\rho_1 + (V_2 - V_b)\rho_2}{V_c} \tag{S15}$$

where V_1 is the reference cell volume, V_2 is the sample cell volume, V_b is the bulk volume of the sample, V_c is the total void volume of the system minus V_b where $V_c = V_1 + V_2 - V_b$.

If the bulk density of the sample is ρ_b and the total mass of the sample is M_s, then the total number of sample particles N is:

$$N = \frac{M_s}{\frac{4}{3}\pi {R_a}^3 \rho_b} \quad \text{(S16)}$$

Based on Darcy's law, the gas flow into a sample Q is:

$$Q = -4\pi R^2 (k_s \frac{\partial p}{\partial r}) N = -\frac{3}{R}\frac{M_s}{\rho_b} k_s \frac{\partial p}{\partial r} \quad \text{(S17)}$$

According to mass conservation and in combination with Eq. (S17), for $t > 0$ and $r = R_a$, we have

$$-\frac{3}{R} V_b K_a c_t \phi_f \frac{\partial p}{\partial r} \rho_s = V_c \frac{\partial \rho_f}{\partial t} \quad \text{(S18)}$$

Substituting Eq. (1C) into Eq. (S18), the boundary condition of Eq. (S10), for ξ =1, is:

$$-\frac{3}{R} V_b K_a \phi_f \frac{\partial \rho_s}{\partial r} = V_c \frac{\partial \rho_f}{\partial t} \quad \text{(S19)}$$

Substituting dimensionless variables into Eq. (S10) yields:

$$\frac{\partial U_s}{\partial \tau} = \frac{\partial^2 U_s}{\partial \xi^2} \quad \text{(S20)}$$

By defining parameter K_c as:

$$K_c = \frac{V_c}{V_b \phi_f} \quad \text{(S21)}$$

the boundary condition of Eq. (S19) becomes:

$$\frac{\partial U_f}{\partial \tau} = -\frac{3}{K_c}(\frac{\partial U_s}{\partial \xi} - \frac{U_s}{\xi}) \quad \text{(S22)}$$

From Eq. (S21), K_c represents the ratio of gas storage capacity of the total void volume of system to the pore volume (including both adsorption and non-adsorption volume) of sample.

The initial condition of Eq. (S20), for $\tau = 0$, is:

when $0 \le \xi < 1, U_s = 0$ (S23)

For $\tau > 0$:

$$\xi = 0, U_s = 0 \quad \text{(S24)}$$

$$\xi = 1, U_s = U_f = 1 \quad \text{(S25)}$$

$$\frac{\partial U_s}{\partial \tau} = \frac{\partial^2 U_s}{\partial \xi^2}, 0<\xi < 1 \quad \text{(S26)}$$

Replacing the Heaviside operator $p = \partial/\partial\tau$ as $p = -s^2$, Eq. (S20) and Eq. (S22) then become:

$$\frac{\partial^2 U_s}{\partial \xi^2} + s^2 U_s = 0\Big|_{U_s=0,\xi=0} \quad \text{(S27)}$$

$$\alpha^2(U_s - 1) = \frac{3}{K_c}\left(\frac{\partial U_s}{\partial \xi} - \frac{U_s}{\xi}\right)\Big|_{\xi=1} \quad \text{(S28)}$$

For these first- and second-order ordinary differential equations, we can solve Eqs. (S27) and (S28) as:

$$U_s = \frac{\alpha^2 \sin\alpha\xi}{\frac{3}{K_c}(\sin\alpha - \alpha\cos\alpha) + \alpha^2 \sin\alpha} \quad \text{(S29)}$$

In Eq. (S29), α_n are the roots of Eq. (S30):

$$\tan\alpha = \frac{3\alpha}{3+\alpha^2 K_c} \quad \text{(S30)}$$

Defining the numerator and denominator of Eq. (S29) as functions $f(\alpha)$ and $F(\alpha)$, U_s can be expressed as:

$$U_s = \underset{\alpha\to 0}{F}\frac{f(\alpha)}{F(\alpha)} + 2\sum_{n=1}^{\infty}\frac{f(\alpha_n)}{\alpha_n F'(\alpha_n)} e^{-{\alpha_n}^2\tau} \quad \text{(S31)}$$

SI2-1: Solution for the Limited K_c Value

Under the condition of limited K_c value, Eq. (S20) is solved with the boundary condition of $0 < \xi < 1$ at time t, and the gas state on the grain surface is initially at equilibrium with the gas outside. Using the Laplace transform, Eq. (S31) is given as (the Laplace transform part can be found in APPENDIX V of Carslaw & Jaeger, 1959) (Brokaw, 1968; Sutherland, 1895):

$$U_s = \frac{\xi K_c}{K_c+1} + 6\sum_{n=1}^{\infty} \frac{\sin \xi\alpha_n}{\sin \alpha_n} \frac{K_c e^{-{\alpha_n}^2 \tau}}{9(K_c+1)+{\alpha_n}^2 {K_c}^2} \qquad \text{(S32)}$$

As the pressure transducer detects the pressure in the reference cell, with the boundary condition $U_f = U_s|_{\xi=1}$, we can calculate U_f as:

$$U_f = \frac{K_c}{1+K_c} + 6\sum_{n=1}^{\infty} \frac{K_c e^{-{\alpha_n}^2 \tau}}{9(K_c+1)+{\alpha_n}^2 {K_c}^2} \qquad \text{(S33)}$$

For a convenient expression of α_n through logarithmic equation, Eq. (S33) can be transformed as:

$$(1-U_f)(1+K_c) = 1 - 6\sum_{n=1}^{\infty} \frac{K_c(1+K_c) e^{-{\alpha_n}^2 \tau}}{9(K_c+1)+{\alpha_n}^2 {K_c}^2} \qquad \text{(S34)}$$

The left side of Eq. (S34) clearly has a physical meaning for the state of gas transport outside the sample, and we define $(1-U_f)(1+K_c)$ as F_f, which is less than, but infinitely close to, 1. Parameter F_f represents (1) the fraction of final gas transfer of V_c which has taken place by time *t*, which can be interpreted as the net change in the density of gas at time *t* to time infinity as Eq. (S35), or (2) as the fractional approach of the gas density to its steady-state in terms of dimensionless variables as Eq. (S36).

$$F_f = \frac{\rho_{p0}-\rho_{pf}}{\rho_{p0}-\rho_{f\infty}} \text{ or} \tag{S35}$$

$$F_f = \frac{1-U_f}{1-U_\infty} = \frac{\rho_{p0}-\rho_{pf}}{\rho_{p0}-\rho_{p2}}(1+K_c) \tag{S36}$$

where for $\tau \to \infty$, the result of U_f and $\rho_{f\infty}$would tend to be the limiting value:

$$U_\infty = U_s = U_f\xi = \frac{\xi K_c}{1+K_c}\Big|_{\xi=1} \tag{S37}$$

$$\rho_{f\infty} = \frac{V_1\rho_1+(V_2-V_s)\rho_2}{V_1+V_2-V_s} = \frac{K_c}{1+K_c}(\rho_{p0}-\rho_{p2})+\rho_{p2} \tag{S38}$$

Thus, Eq. (S34) can be expressed as:

$$F_f = 1-6\sum_{n=1}^{\infty}\frac{K_c(1+K_c)e^{-\alpha n^2\tau}}{9(K_c+1)+\alpha_n{}^2K_c{}^2} \tag{S39}$$

For calculating the permeability, Eq. (S39) can be linearized as a function of time as there are no variables other than the exponential part:

$$ln(1-F_f) = f_1 - s_1 t \tag{S40}$$

where f_1 is the intercept for the y-axis of function (S40):

$$f_1 = ln[\frac{6K_c(1+K_c)}{9(1+K_c)+\alpha_1{}^2K_c{}^2}] \tag{S41}$$

The slope s_1 can be captured by the fitted line of the linear segment, and α_1 is the first solution of Eq. (S30):

$$s_1 = \frac{\alpha_1{}^2K_a}{R_a{}^2} \tag{S42}$$

Thus, the permeability can be calculated as:

$$k = \frac{R_a{}^2\mu c_t\phi_f s_1}{\alpha_1{}^2} \tag{S43}$$

SI2-2: Solution for K_c Goes to Infinity

When V_c has an infinite volume compared to the void volume in a sample, which means that the density of gas in V_c would be kept at ρ_{p0}, and α would approach $n\pi$ in Eq. (S30), then Eq. (S32) can be transformed as:

$$U_s = \xi + \frac{2}{\pi}\sum_{n=1}^{\infty}(-1)^n \frac{\sin n\pi\xi}{n} e^{-(n\pi)^2\tau} \quad \text{(S44)}$$

In this situation, $U_f = 1$, and as the gas density would be maintained at the initial state at ρ_{p0}, it would be a familiar case in diffusion kinetics problems with the uptake rate of F_f to be expressed as F_s in V_b (Barrer, 1941):

$$F_s = \frac{\rho_{sav}}{\rho_{s\infty}} \quad \text{(S45)}$$

where ρ_{sav} is the average value of ρ_{sr} in the grain, and $\rho_{s\infty}$ is the maximum value of ρ_{sr}:

$$\rho_{sr} = \rho_{ps} - \rho_{p2}, \quad \rho_{s\infty} = \rho_{p0} - \rho_{p2} \quad \text{(S46)}$$

The value of ρ_{sr} in the grain is:

$$\rho_{sav} = \frac{3}{R^3}\int_0^R \rho_{sr} r^2 \, d\, r \quad \text{(S47)}$$

Then F_s becomes:

$$F_s = \frac{3}{R^3}\int_0^R \frac{U_s}{\xi} r^2 \, d\, r \quad \text{(S48)}$$

Substituting Eq. (S44) into Eq. (S48), we can calculate:

$$F_s = 1 - \frac{6}{\pi^2}\sum_{n=1}^{\infty}\frac{e^{-(n\pi)^2\tau}}{n^2} \quad \text{(S49)}$$

Similar to Eq. (S39), Eq. (S49) can also be linearized to calculate the permeability in τ from the fitted slope. For $\tau \geq 0.08$, Eq. (S49) can be reduced as:

$$F_s = 1 - \frac{6}{\pi^2}e^{-\pi^2\tau} \quad \text{(S50)}$$

When t is small enough (for $\tau \leq 0.002$), Eq.(S49) can be transformed into Eq. (S51).

$$F_s = 6\sqrt{\frac{\tau}{\pi}} \quad \text{(S51)}$$

As F_s is a special solution of F_f with the case of K_c goes to infinity, we can arrive at:

$$F_s = F_f = (1 - U_f)(1 + K_c) \quad \text{(S52)}$$

For testing the ultra-low permeability rocks using granular samples whenK_c goes to infinity, Eq. (S50) and Eq. (S51) can be selected using different τ values.

From the fitted slope s_2 of function $ln(1 - F_s)$ from Eq. (S50), we can then derive the permeability:

$$k = \frac{{R_a}^2\mu c_t\phi_f s_2}{\pi^2} \quad \text{(S53)}$$

The results of Eq. (S53) are very similar to Eq. (S43) as the first solution for Eq. (S30) is very close to π.

From the fitted slope s_3 of function ${F_s}^2$ from Eq. (S51), we can derive the permeability:

$$k = \frac{\pi {R_a}^2 \mu c_t \phi_f s_3}{36} \quad \text{(S54)}$$

SI3. A Case of Data Processing for GPT

We show here an illustration of the data processing procedure for the GPT with a molecular sieve sample (https://www.acsmaterial.com/molecular-sieves-5a.html). This material consists of grains of 2 mm in Diameter with a porosity of 26.28%, and a uniform pore-throat size of 5Å in Diameter, with a particle density of 2.96 g/cm^3. For a 45 g sample, the K_c value is 19.4 from Eq. (S21), and therefore 4.9% of the density ratio $(1 - K_f)$ is available for mass transfer from Eq. (1K).

The experimental data were captured under a strict temperature control and unitary-gas environment, along with a precise measurement of barometric pressure. The experiment was run twice, and after the data were collected, 1) we made a rough evaluation of the "Penetration Zone" of this sample based on Figs. 5-6. For this molecular sieve sample, the "Penetration Zone" is shown in Fig. S1, and the mass transfer in unit time more conforming to a linear state (shown as Fig. 5) over a large time range, especially at 100-300s; 2) data in the selected range (100-300s) were fitted respectively for the slope from Fig.

S2, then slopes were compiled in Table SI3-1; 3) permeabilities were calculated using the slope of the fitted curve, and all results for LLT, ILT and IET are also shown in Table SI3-1; 4) the results were checked with their dimensionless times to verify whether the early- or late-time solutions were used correctly. Table SI3-1 clearly shows that the results of IET should be selected for this sample, as the dimensionless time is less than 0.024. Note that the data fluctuation shown here was from a high resolution ($\pm$0.1% for 250 psi) pressure sensor without undergoing a smoothing process; meanwhile, for data in the 100-200, 200-300, and 300-400 seconds of experimental duration, 100, 200, and 300 seconds respectively were used to calculate the dimensionless times for the results in Table SI3-1.

In addition, the validity of the permeability obtained needs to be verified by using the time interval employed in data fitting and the calculated permeability results to calculate the τ (Table SI3-1). If the dimensionless time is less than 0.024 (as occurred for the case of molecular sieve), the IET solution is selected; if the dimensionless time is greater than 0.024 and K_c is greater than 10, the ILT solution is used; if τ is greater than 0.024 and K_c is less than 10, then the LLT solution is employed. However, for sample sizes smaller than 1.27 mm, Conflicting Results (described in Table 1) occur, and results from this situation are not recommended due to poor data quality.

840 Table SI3-1. Permeability results of molecular sieve from LLT, IET and ILT

Fitting range (s)	LLT (m^2)	τ - LLT	IET(m^2)	τ - IET	ILT (m^2)	τ -ILT	Slope-LLT	Slope-IET	Slope-ILT
100-200	5.60E-22	0.004	1.02E-21	0.007	5.00E-22	0.003	0.0004	0.0007	0.0004
200-300	4.20E-22	0.006	5.81E-22	0.008	3.75E-22	0.005	0.0003	0.0004	0.0003
300-400	2.80E-22	0.006	4.36E-22	0.009	2.50E-22	0.005	0.0002	0.0003	0.0002

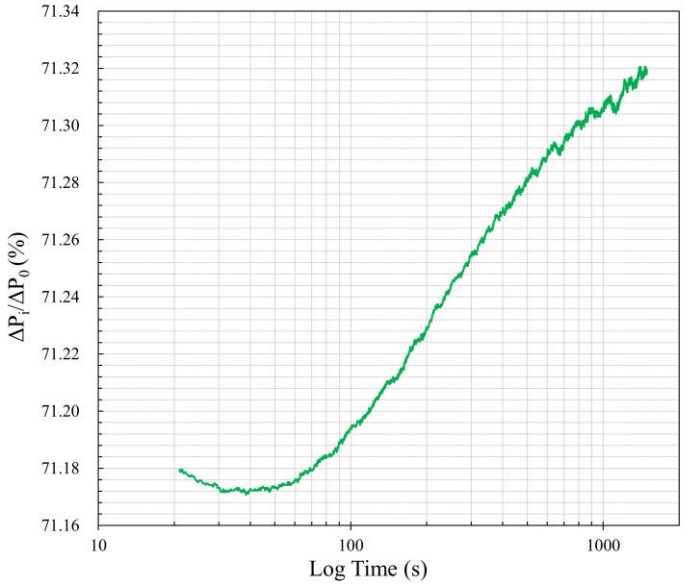

841

842 Fig. S1. Unit pressure change varying with experimental time.

843

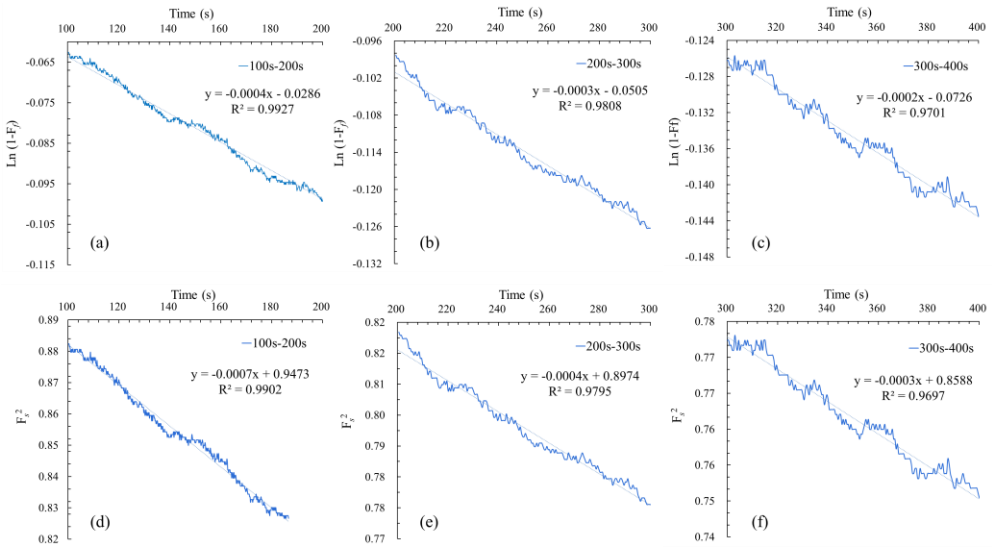

844

Fig. S2. Fitted slopes for each solution; (a) to (c) are results of LLT and ILT, while (d) to (f) of IET.

SI4. Equipment and samples

The experimental setup in the GPT presented in this study is based on the GRI-95/0496 protocols (Guidry et al., 1996) and the SMP-200 guidelines from Core Laboratories with the gas expansion approach (shown in Fig. S3). In this work, gases (He, Ar, N_2, or CO_2) with different molecular sizes and sorption capacities were tested using two shale core samples (X1, X2) from an oil-producing lacustrine formation in the Songliao Basin, China. X1 is used for sample size study where X2 used for experiment with different gas. Also, we used the molecular sieve to exhibit the practical utilization of the GPT method in SI3. We gently crushed the intact samples with mortar and ground to different granular sizes from 0.34 mm to 5.18 mm through a stack of sieves (named here as Size X: 8 mm to #8 mesh; GRI+: #8-#12 mesh; Size A: #12-#20 mesh; GRI: #20-#35 mesh; Size B: #35-#80 mesh).

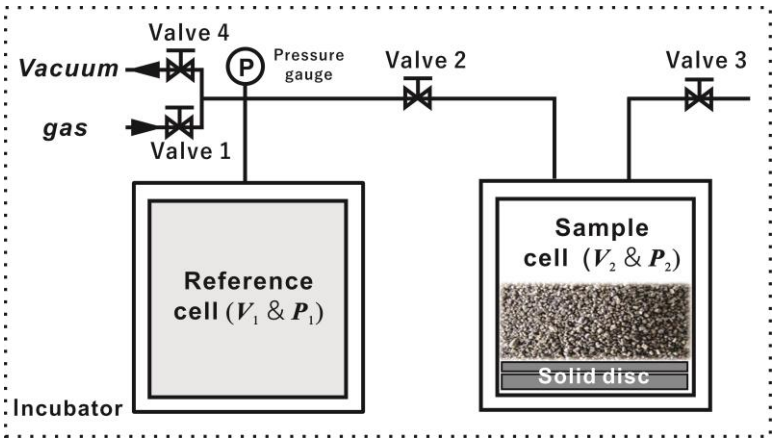

Fig. S3. Scheme of the GPT experiment for granular samples with all the cells and supplies placed inside an incubator for temperature control.

After loading each sample, related accessories (e.g., solid discs or balls for volume control; and hence porosity, sample mass, and solution-related) were placed below samples inside the cell (Fig. S3). Next, valves 1 and 3 were closed, then valves 2 and 4 were opened for air evacuation. Using a precise pressure gauge connected to the reference cell shown in Fig. S3 we monitored changes in the pressure. The evacuation time typically lasted at least 15-30 min, and then the system was allowed to stabilize for another 15 min. As the moisture content of the samples significantly influences the final vacuum, the samples were placed into the sample cell immediately after removal from the drying oven set at 60ºC for two days and cooling in a low-humidity desiccator.

The experiments were conducted at the temperature of 35°C by placing the SMP-200 inside an incubator equipped with a high precision temperature-

875 humidity sensor to monitor changes. This is to ensure that the system
876 temperature was always stable (0.05°C over at least 45 mins of experimental
877 duration). For temperature monitoring, after evacuation, we closed valves 3
878 and 4 followed by opening valves 1 and 2 (shown in Fig. S3) and monitoring
879 the heat convection and conduction in the system with the pressure gauge.
880 Normally, the sample was placed inside the sample cell in less than 30 sec
881 after opening the incubator and remained at least 45 min for the gas pressure
882 to stabilize before the pressure decay test. After the pressure was stabilized
883 (0.005 psi for an experimental pulse pressure of 200 psi), it was deemed that
884 there was no appreciable additional flow due to temperature variation in the
885 system, as indicated by the rebound of the pressure decay curve. After reaching
886 a unitary gas condition and stable temperature in the GPT experiment, valves
887 2 and 4 were closed, and the reference cell was filled with the probing gas
888 (mostly non-reactive helium) at 200 psi. Valve 2 was then opened to release
889 the pressure in the reference cell into the void volume in the sample cell, and
890 the pressure decay for both reference and sample cells were recorded over time.

891 **SI5. Experimental conditions**

892 We performed leakage tests by measuring the pressure variation with non-
893 porous solids, such as steel balls, as any leakage would cause pressure
894 variations and, accordingly, errors in permeability measurements of tight

porous samples (Heller et al., 2014). Before the data from porous samples were analyzed, the leakage pressure from the steel ball experiment was subtracted from the sample data to correct the modest (<5% of the pressure levels used for permeability analyses) leakage effect.

The need for a unitary gas environment (a single gas used in both reference and sample cells) is needed to successfully measure permeability via the GPT method. The relative movement of gas molecules in the mass transfer process is driven by the gas density gradient in the system. During gas transport, the pressure variance was recorded and used to obtain the permeability coefficient. However, when the gas in both cells is different, e.g., helium in the reference and air in the sample cells, the mathematical analysis requires a complicated correction accounting for the mean molar mass and the average gas dynamic viscosity of the gas mixture. In this study, we present the calculation with the viscosity of mixed gases for the GPT in the SI1. Since the mixed gas environment is not recommended, air evacuation should be used for a well-controlled unitary gas environment in the GPT.

A stable temperature is another critical point to ensure the success of the GPT experiment. A sensitive pressure transducer in combination with the ideal gas law, used to establish the relationship between pressure and gas volume change, would be a much more convenient and precise way than the gas flow

meter to determine the gas permeability considering the measurement accuracy. According to Amonton's law (Gao et al., 2004), the kinetic energy of gas molecules is determined by the temperature, and any changes would alter the molecular collision force causing a pressure variation and a volumetric error. The GPT experiments were run two or three times on the same sample, and the sample skeletal density at the end of the experiment were obtained to check the overall indication of leakage and temperature control. The experimental data with relatively large and stable skeletal density (mostly the last run, from small but appreciable pressure change to reach stable values) were used.

Appendix References:

Barrer, R.M., 1941. Diffusion in and through solids, Рипол Классик.

Brokaw, R.S., 1968. Viscosity of gas mixtures, National Aeronautics and Space Administration.

Carslaw, H.S., Jaeger, J.C., 1959. Conduction of heat in solids.

Gao, J., Luedtke, W.D., Gourdon, D., Ruths, M., Israelachvili, J.N., Landman, U., 2004. Frictional forces and Amontons' law: from the molecular to the macroscopic scale, ACS Publications.

Guidry, K., Luffel, D., Curtis, J., 1996. Development of laboratory and petrophysical techniques for evaluating shale reservoirs. Final technical report, October 1986-September 1993, ResTech Houston, Inc., TX (United States).

Haskett, S.E., Narahara, G.M., Holditch, S.A., 1988. A method for simultaneous determination of permeability and porosity in low-permeability cores. SPE formation evaluation 3(03), 651-658.

Heller, R., Vermylen, J., Zoback, M., 2014. Experimental investigation of matrix permeability of gas shalesExperimental Investigation of Matrix Permeability of Gas Shales. Aapg Bull. 98(5), 975-995.

Sutherland, W., 1895. XXXVII. The viscosity of mixed gases. The London, Edinburgh, and Dublin Philosophical Magazine and Journal of Science 40(246), 421-431.